Received: 29 April 2023 | Revised: 6 July 2023 | Accepted: 6 July 2023

DOI: 10.1002/eom2.12394

RESEARCH ARTICLE

EcoMat FUNCTIONAL MATERIALS FOR GREEN ENERGY AND ENVIRONMENT WILEY

CoNiFe-layered double hydroxide decorated Co-N-C network as a robust bi-functional oxygen electrocatalyst for zinc-air batteries

Yasir Arafat[1,2] | Yijun Zhong[1] | Muhammad R. Azhar[2] | Mohammad Asif[3] | Moses O. Tadé[1] | Zongping Shao[1]

[1]WA School of Mines: Minerals, Energy and Chemical Engineering (WASM-MECE), Curtin University, Perth, Western Australia, Australia

[2]School of Engineering, Edith Cowan University, Joondalup, Western Australia, Australia

[3]Department of Chemical Engineering, King Saud University, Riyadh, Saudi Arabia

Correspondence
Zongping Shao, WA School of Mines: Minerals, Energy and Chemical Engineering (WASM-MECE), Curtin University, Perth, WA 6102, Australia.
Email: zongping.shao@curtin.edu.au

Funding information
Australian Research Council, Grant/Award Numbers: DP200103315, DP200103332, DP220103669

Abstract

Rechargeable zinc-air batteries (ZABs) are cost-effective energy storage devices and display high-energy density. To realize high round-trip energy efficiency, it is critical to develop durable bi-functional air electrodes, presenting high catalytic activity towards oxygen evolution/reduction reactions together. Herein, we report a nanocomposite based on ternary CoNiFe-layered double hydroxides (LDH) and cobalt coordinated and N-doped porous carbon (Co-N-C) network, obtained by the in-situ growth of LDH over the surface of ZIF-67-derived 3D porous network. Co-N-C network contributes to the oxygen reduction reaction activity, while CoNiFe-LDH imparts to the oxygen evolution reaction activity. The rich active sites and enhanced electronic and mass transport properties stemmed from their unique architecture, culminated into outstanding bi-functional catalytic activity towards oxygen evolution/reduction in alkaline media. In ZABs, it displays a high peak power density of 228 mW cm^{-2} and a low voltage gap of 0.77 V over an ultra-long lifespan of 950 h.

KEYWORDS

layered double hydroxides, metal organic framework (MOF), oxygen electrocatalysis, zeolite imidazole framework (ZIF), zinc-air battery

1 | INTRODUCTION

Current world experiences quickly expanded consumption of fossil fuels due to the rapid global population growth and economic progress,[1,2] while their non-renewable and carbon-rich nature and rich impurity bring negative impacts on our ecosystem and environment and also serious concerns about the sustainability of energy supply.[3,4] In 2015, world leaders committed to an urgent call for 17 actions named as the UN sustainable development goals, including ensuring the accessible and clean energy and doubling the global rate of energy efficiency by 2030.[5] Likewise, the nations agreed to Paris Agreement in late 2015 to control the global temperature rise to 1.5°C and to limit the global CO_2 atmospheric concentrations to 450 ppm by 2050.[3] To reach these targets, the sustainable energy resources, such as solar, wind, and hydro etc., will play an important role. Nevertheless, their intermittent

nature disrupts the grid's operation, therefore it is vital to integrate some reliable energy storage systems for the electricity generation from these renewable energy resources. Zinc batteries, being the oldest energy-storage systems, hold a great promise to develop a sustainable society. In particular, rechargeable zinc-air batteries (ZABs), which use the metal anode and oxygen as cathode active material, are prioritized over other batteries because of their low cost, environmental benignity, high theoretical energy density, and in-built safety.

The working principle of ZABs is based on the oxygen redox reactions: oxygen evolution reaction (OER) during charge and oxygen reduction reaction (ORR) during discharge at the air electrode. Unfortunately, state-of-the-art ZABs demonstrate sluggish OER/ORR kinetics for their air electrodes, leading to a large voltage gap during the charging-discharging cycle, thereby causing a low round trip efficiency. To enhance the round-trip efficiency, it is critical to develop proper electrocatalysts that should show excellent bi-functionality (high catalytic activity for both ORR and OER) and durability. The challenge in the development of air electrodes for rechargeable ZABs is that ORR and OER typically happen at different active sites and proceed through different reaction pathways, thus a single material may be difficult to realize high activity for both ORR and OER.[6,7] Instead, the development of some composite electrocatalysts with separated active sites for ORR as well as OER is a more efficient strategy towards the enhancement of ZABs performance.

Compounds based on some earth-abundant metals, including transition metal oxides, nitrides, sulfides, phosphides, and layered double hydroxides, have been well established as favorable electrocatalysts for OER in alkaline media.[8,9] Among them, layered double hydroxides (LDHs) are of particular interest because of their intriguing activity, cost-effectiveness, chemical versatility, structural flexibility, and low toxicity.[10,11] LDHs are 2D lamellar crystals denoted by $[M^{2+}_{1-x}M^{3+}_{x}(OH)_2]^{x+}(A^{n-})_{x/n}\cdot mH_2O$, wherein M^{2+} and M^{3+} refer to the bivalent and trivalent cationic host layers respectively. A^{n-} are the anions intercalated between the host layers to balance the positively charged layers[8,12,13] and solvent molecules whereas x (Molar ratio of $M^{3+}/(M^{2+}+M^{3+})$) usually ranges between 0.17 and 0.33. Trivalent metal cations (such as Fe^{3+}, Al^{3+}, or Ga^{3+}) substitute partially isomorphic bivalent metal cations (Fe^{2+}, Co^{2+}, and Ni^{2+}), while coordinating octahedrally by OH^-.[14] The intercalated ions are usually organic or inorganic anions (such as RCO_2^-, CO_3^{2-}, Cl^-, SO_4^{2-}, and NO_3^-). Each hydroxyl is oriented between the layers and tends to establish hydrogen bonding with water molecules or with intercalated anions.[11]

Since the first ever discovery of favorable activity of ZnCo LDHs as OER catalyst, various LDHs based on Co, Ni, Fe, Mn, W and Cr have been investigated as potential OER and/or ORR electrocatalysts.[15–19] Among them, NiFe-LDHs have been demonstrated as remarkable OER electrocatalysts.[9,20,21] To further enhance the OER performance of NiFe-LDHs, it is vital to modulate their electronic structure. On the other hand, the low electronic conductivity of LDHs is the major bottleneck in their application to energy devices.[11,13,22] It was found that the introduction of a third metal element with high valence, for instance, cobalt, could effectively promote the electronic transport, thus leading to improve the electrocatalytic activity of the NiFe-LDHs, outperforming the mono-metallic or bi-metallic LDHs.[19,23,24]

On the other hand, metal organic frameworks (MOFs) are another type of functional materials which have received considerable attention for their unique mesoporous structure, which can greatly facilitate mass transfer during the electrocatalytic reaction.[25] Zeolitic imidazolate frameworks (ZIFs) are recognized as a sub-class of MOFs. Of note, the pyrolysis of ZIF-67 can yield cobalt coordinated, N-rich and porous carbonaceous frames (Co-N-C), which display large surface area, excellent electrical conductivity and favorable ORR activity.[26–28] So ZIFs have been extensively employed as precursors to prepare metal-doped carbon materials as ORR electrocatalysts.[29]

Herein, we propose a composite electrode with unique architecture and synergistic effect for ZABs by coupling the LDHs that possess high OER catalytic activity while poor electronic conductivity with ZIF-67 derived Co-N-C that shows the porous structure, high electronic conductivity and superior ORR activity, resulting in excellent bi-functionality (ORR/OER) and durability. The catalyst was facilely prepared via a hydrothermal method and the doping of a third element (Co) into CoNiFe-LDH was conducted to modify the electronic structure of LDH. It not only promoted the electronic conductivity but also lowered the onset potential for oxygen evolution activity. A synergy between the Co-N-C and the ternary CoNiFe-LDH was developed to endorse the catalyst with enhanced bi-functional activity for oxygen electrocatalysis in an alkaline solution. When the bi-functional air electrode was integrated into ZABs, it produced a small voltage gap of 0.77 V, a high peak power density (PPD) of 228 mW cm^{-2}, and a remarkable stability over 950 h, making it highly promising for practical use.

2 | RESULTS AND DISCUSSION

2.1 | Characterizations of the catalyst

Figure 1A illustrates schematically the synthesis procedure of the Co-N-C@CoNiFe-LDH nanocomposite.

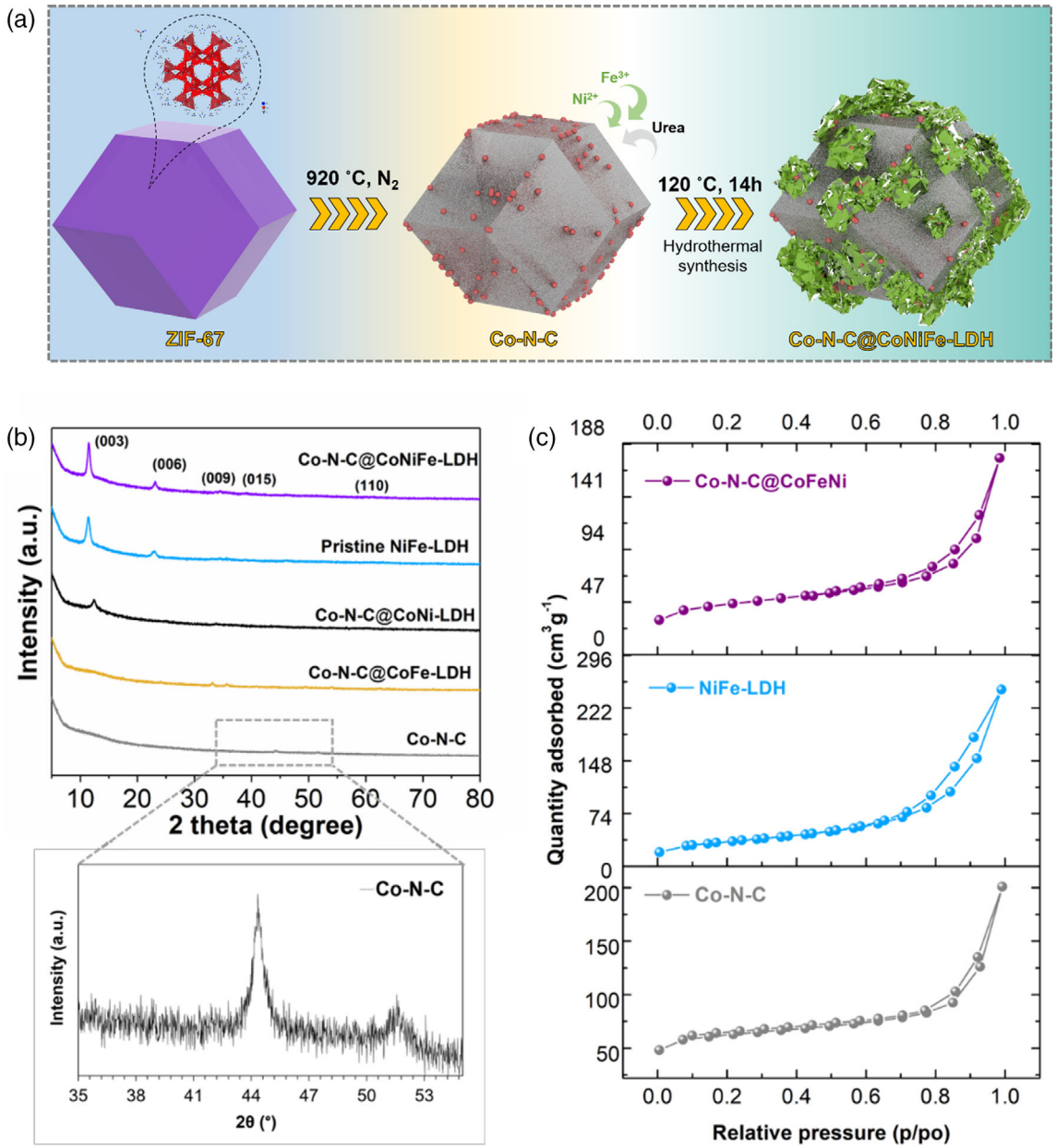

FIGURE 1 (A) A schematic description of synthesis of Co-N-C@CoNiFe-LDH. (B) X-ray diffraction patterns of Co-N-C, pristine NiFe-LDH, Co-N-C@ CoNiFe-LDH, Co-N-C@CoNi-LDH and Co-N-C@CoFe-LDH samples. (C) N_2-sorption isotherms of Co-N-C, pristine NiFe-LDH, Co-N-C@ CoNiFe-LDH.

During the hydrothermal treatment, the hydrolysis reaction of Fe^{3+}/Ni^{2+} ions happened to generate protons, which induced the etching of Co-N-C to release partial Co^{2+} ions into the solution near the Co-N-C surface, and some Co^{2+} ions in the solution were oxidized to Co^{3+} ions by oxidizing agents (O_2 and NO_3^- ions). Such Co^{2+}/Co^{3+} species finally co-precipitated with Ni^{2+}, Fe^{3+} and OH^- ions to form a thin layer of CoNiFe-LDH, which decorated over the Co-N-C surface (Equations 1–4).

$$Ni^{2+} + 2H_2O \rightarrow Ni(OH)_2 + 2H^+, \quad (1)$$

$$Fe^{3+} + 3H_2O \rightarrow Fe(OH)_3 + 3H^+, \quad (2)$$

$$Co^{2+} + 2H_2O \rightarrow Co(OH)_2 + 2H^+, \quad (3)$$

$$Ni^{2+} + Co^{3+} + Fe^{3+} + xH_2O \rightarrow CoNiFe(OH)_x + xH^+. \quad (4)$$

To confirm the LDH structure and its phase transformation during the synthesis, x-ray diffraction (XRD) of the various samples was conducted with the related patterns illustrated in Figures 1B, S1, and S2. For the

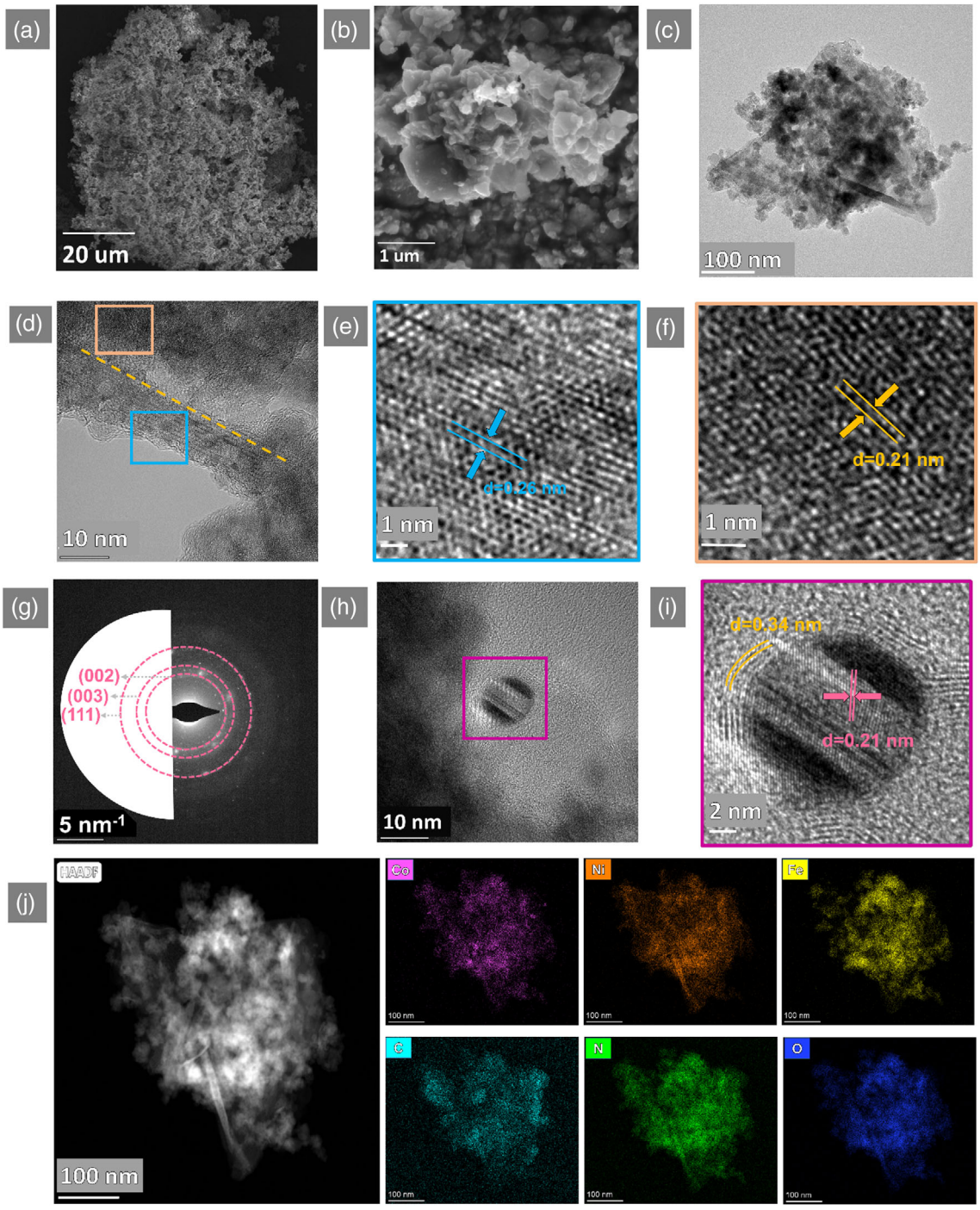

FIGURE 2 (A,B) Scanning electron microscopy images. (C) High-resolution transmission electron microscopy (HRTEM) images, and (D–F) HRTEM images of Co-N-C@ CoNiFe-LDH, (g) selected area electron diffraction (SAED), (H,I) HRTEM images of Co-N-C core, and (J) HAADF-STEM images and its corresponding element mapping.

pristine NiFe-LDH, the diffraction peaks at 2-theta of 11.37°, 22.94°, 34.4°, 38.9° and 60.6° can be indexed well to the (003), (006), (009), (015), and (110) crystal planes corresponding to LDHs, implying the successful formation of layered double hydroxide phases. In the case of Co-N-C@CoNiFe-LDH, the major diffraction peaks representing LDH of (003), (006) planes slightly shifted to the higher diffraction angles in contrast with the pristine NiFe-LDH, which is in good agreement with the smaller size of cobalt than Ni and Fe, suggesting the partial incorporation of Co species into the Ni-Fe lattice. The major peaks became sharp and intense, which further reinforced the evolution of ternary FeCoNi-LDH. The incorporation of Co species into the Ni-Fe layer resulted in the

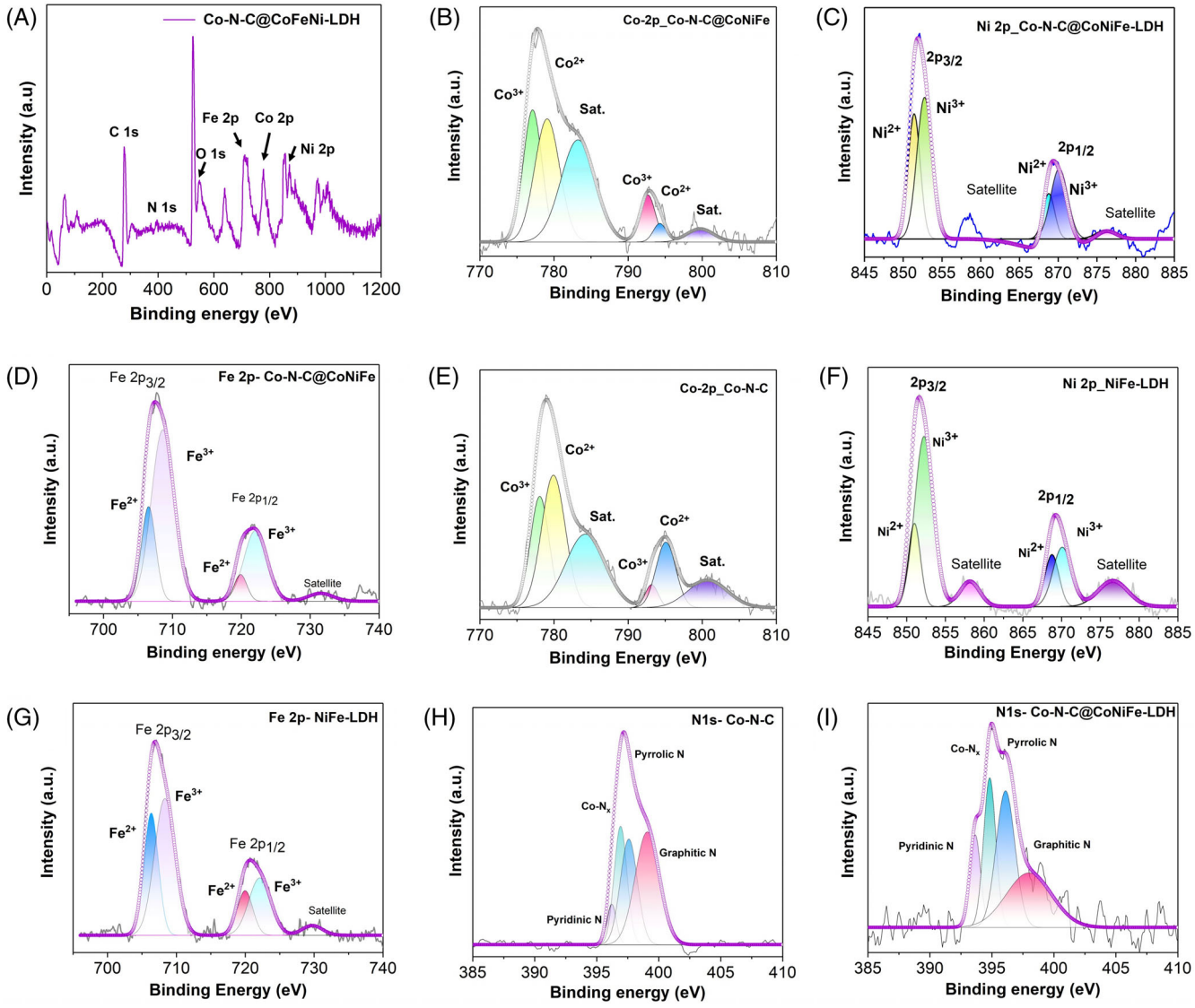

FIGURE 3 (A) XPS survey spectrum of Co-N-C@CoNiFe-LDH, High-resolution XPS spectrum of Co-N-C@CoNiFe-LDH for (B) Co 2p, (C) Ni 2p (D) Fe 2p, (I) N 1 s, high-resolution XPS spectrum of Co-N-C for (E) Co 2p (H) N1s, High-resolution XPS spectrum of NiFe-LDH for (F) Ni 2p and (G) Fe 2p.

rearrangement of the electronic structure of the LDH, which may have an impact on the OER catalytic activity. In addition to the above diffraction peaks, three new diffraction peaks at 44.2°, 52.1° and 75.6° were also observed, which can be indexed (111), (200), (220) reflections of Co and N doped carbon (Co-N-C). Clearly, the doped cobalt into NiFe-LDH should be originated from the Co-N-C species that is, cobalt species were partially transformed from Co-N-C into CoNiFe-LDH during the hydrothermal treatment.

The surface area of the material is important for the infiltration of electrolyte and the exposure of active sites. BET surface area was evaluated to determine the influence of Co-N-C substrate in exposing the CoNiFe-LDH active sites (Figure 1C). N_2-physisorption isotherms displayed the type IV isotherm, representative of the mesoporous structure together with H_4-type hysteresis loop. It suggests the surface area of LDH-based composite significantly enhanced after the in-situ growth of NiFe-LDH over the Co-N-C substrate in comparison with pristine NiFe-LDH (Table S1). The morphology of Co-N-C@CoNiFe-LDH was observed by scanning electron microscopy (SEM) and transmission electron microscopy (TEM). The derived Co-N-C partially lost the typical dodecahedron morphology of ZIF-67 (as shown in Figure S3a,b), followed by the pyrolysis and hydrothermal treatment (Figure 2A–C). The morphology of Co-N-C@ CoNiFe-LDH was further elaborated on the atomic scale by high-resolution TEM (HRTEM). It was interesting to observe the distinct features at the edges and the

core that is, the lattice fringes at the edges depict the lattice spacing of 0.26 nm, attributing to the LDHs while it is 0.21 nm on the core, corresponding to the Co species (Co-N-C) as shown in Figure 2D–F. Selected area electron diffraction (SAED) displayed the diffraction planes (002), (003) and (111), corresponding to graphitic carbon, CoNiFe-LDH and metallic cobalt species, respectively, as shown in Figure 2G. Moreover, the cobalt metallic species were surrounded by the graphitic carbon Figure 2H,I. The high angle annular dark-field (HAADF) image together with elemental mapping revealed the uniform dispersion of Ni and Fe and Co species for the formation of ternary CoNiFe-LDH over Co-N-C, as shown in Figures 2J and S3c.

To unravel the chemical state and charge transfer of the as-synthesized materials, x-ray photoelectron spectroscopy (XPS) analysis was conducted (Figure 3). The survey spectra of Co-N-C@CoNiFe-LDH displayed the corresponding peaks of Co, Ni, Fe, C, N, and O concomitantly as shown by Figure 3A, which is in line with the EDS results. Co 2p spectrum associated with Co-N-C@CoNiFe-LDH and Co-N-C may be divided into Co $2p_{3/2}$, Co $2p_{1/2}$ and satellite peaks as shown in Figure 3B,E, respectively. These peaks were further deconvoluted into Co^{3+} and Co^{2+} peaks. It is obvious that Co 2p peaks (778.8 eV) in Co-N-C@CoNiFe-LDH negatively shifted in contrast with Co-N-C, indicating the high valence state of Co (i.e. Co^{3+}). It ratifies the presence of trivalent cobalt ions in the Co-N-C@CoNiFe-LDH composite.[30] It suggests that some of Co^{2+} ions were oxidized to Co^{3+} after the CoNiFe LDH formation. Such high valence Co^{3+} species might probably contribute to the OER activity, which will be discussed later. It is worth noticing that Ni 2p and Fe 2p peaks in Co-N-C@CoNiFe-LDH were positively shifted as compared to the peaks in the pristine NiFe-LDH (Figure 3C,F,D,G). This spectroscopic difference implies the strong electronic interaction at the heterojunction of Co-N-C and CoNiFe-LDH in contrast with the NiFe-LDH, which endowed to the intimate contact between Co-N-C surface and the ternary LDH that was embedded over the carbon surface.[31] The concomitance of Ni, Fe and Co might also be helpful to optimize the redistribution of π-symmetry electrons, which is favorable for the adsorption/desorption of the O_2 species.[32] Moreover, graphitic and pyridinic-N similar to Co-N-C in Co-N-C@CoNiFe-LDH also effectively tuned the electron density of carbon atoms (Figure 3H,I). According to C 1 s spectrum, Co-N-C and Co-N-C@ CoNiFe-LDH consisted of sp^2 and sp^3-hybridized C–C bonds, besides C–N (Figure S4). The proportion of sp^3-hybridized C–C bonds, ascribing to graphitic carbon, was significantly increased in case of Co-N-C@ CoNiFe-LDH.[2] Thus, the variation in the binding energy revealed the electrons transfer from Co-N-C to NiFe-LDH. The redistribution could optimize the electronic configuration of the heterogeneous interface to influence the intermediate adsorption energies, so as to promote the ORR/OER redox reactions.

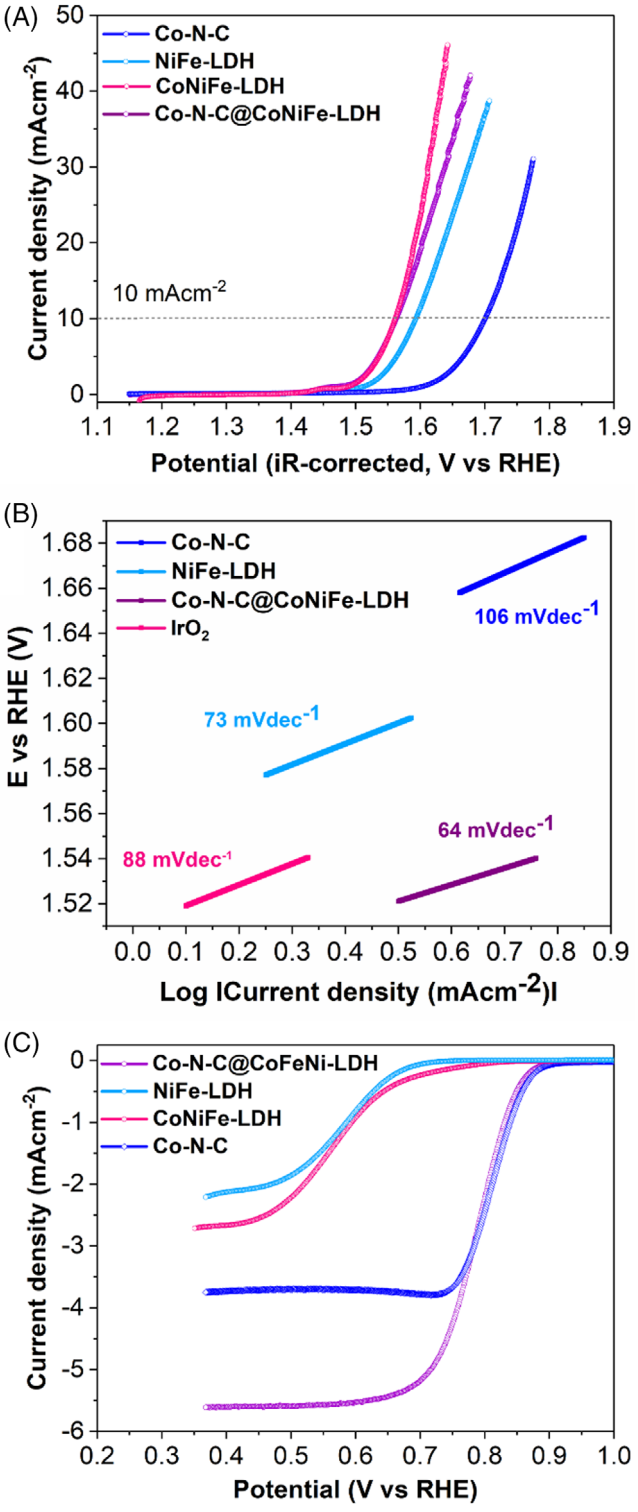

FIGURE 4 Oxygen evolution reaction (OER) polarization curves of (a) NiFe-LDH, CoNiFe-LDH, Co-N-C@ CoNiFe-LDH, and Co-N-C. (B) Tafel slopes. (C) ORR polarization curves of Co-N-C@ CoNiFe-LDH, NiFe-LDH, CoNiFe-LDH, and Co-N-C.

2.2 | Electrochemical performance

The electrocatalytic activities of oxygen redox were first studied through linear sweep voltammograms (LSV) using the three-electrode system in an O_2-saturated alkaline solution. Generally, OER activity of electrocatalysts is determined by evaluating the potential at 10 mA cm^{-2} ($E_j = 10$ mA cm^{-2}). Among the various catalysts, Co-N-C@CoNiFe-LDH and CoNiFe-LDH exhibited the comparable and the lowest potential of 1.55 V versus RHE, superior to the NiFe-LDH (1.59 V) and precious metal-based IrO_2 as shown in Figures 4A and S5. On the other hand, an anodic peak or hump appeared at around 1.41 V, which is a characteristic of the oxidation activity of Co^{2+}/Co^{3+} and Ni^{2+}/Ni^{3+}. Moreover, the catalytic OER performance of Co-N-C and other bimetallic catalysts, such as Co-N-C@CoNi-LDH and Co-N-C@CoFe-LDH, was also significantly lower as compared to the optimal Co-N-C@ CoNiFe-LDH catalyst (Figure S5).

The superior performance of Co-N-C@ CoNiFe-LDH in contrast with pristine NiFe-LDH may be associated with the activation of NiOOH and CoOOH phases in the composite. Actually, the stronger covalency between Ni3d–O2p and Co3d–O2p modulated the electronic structure. As a result, Co-N-C@ CoNiFe-LDH displayed the pre-oxidation (Ni^{2+}/Ni^{3+} and Co^{2+}/Co^{3+}) as well as lower onset potential in contrast with the pristine NiFe-LDH.[33,34] It implies that Co^{2+}/Co^{3+} significantly contributed to promote the oxidation (Ni^{2+} to Ni^{3+}) to form the NiOOH and CoOOH at a relatively lower potential. On the other hand, pristine NiFe-LDH demonstrated the weak oxidation peaks of Ni^{2+} to Ni^{3+}. Thus, the OER activity of Co-N-C@ CoNiFe-LDH was enhanced by the activation of NiOOH phase as influenced by the symbiotic charge transfer effect between Co^{3+} and N-doped carbon species. More importantly, Co^{3+} species might enhance the electrophilicity, which promoted the reaction between adsorbed O atoms and OH^- anions for the formation of such –OOH species.[24]

To get better the insights into OER kinetics, corresponding Tafel slopes of LSV curves were probed as shown by Figure 4B. Co-N-C@ CoNiFe-LDH displayed the Tafel slope of 64 mV dec^{-1}, which was smaller than the pristine NiFe-LDH (73 mV dec^{-1}) and precious metal-based commercial IrO_2 (88 mV dec^{-1}) catalyst. On the other hand, the Tafel slope of bimetallic-based LDH catalysts (e.g. Co-N-C@CoNi-LDH and Co-N-C@CoFe-LDH) were larger in contrast with the ternary Co-N-C@ CoNiFe-LDH catalyst (Figure S6). The small value of the Tafel slope of optimal catalysts is indicative of a change in the reaction control step, leading to the favorable OER kinetics of Co-N-C@ CoNiFe-LDH. Thus, the small value of the Tafel slope is the intrinsic property of the catalyst,

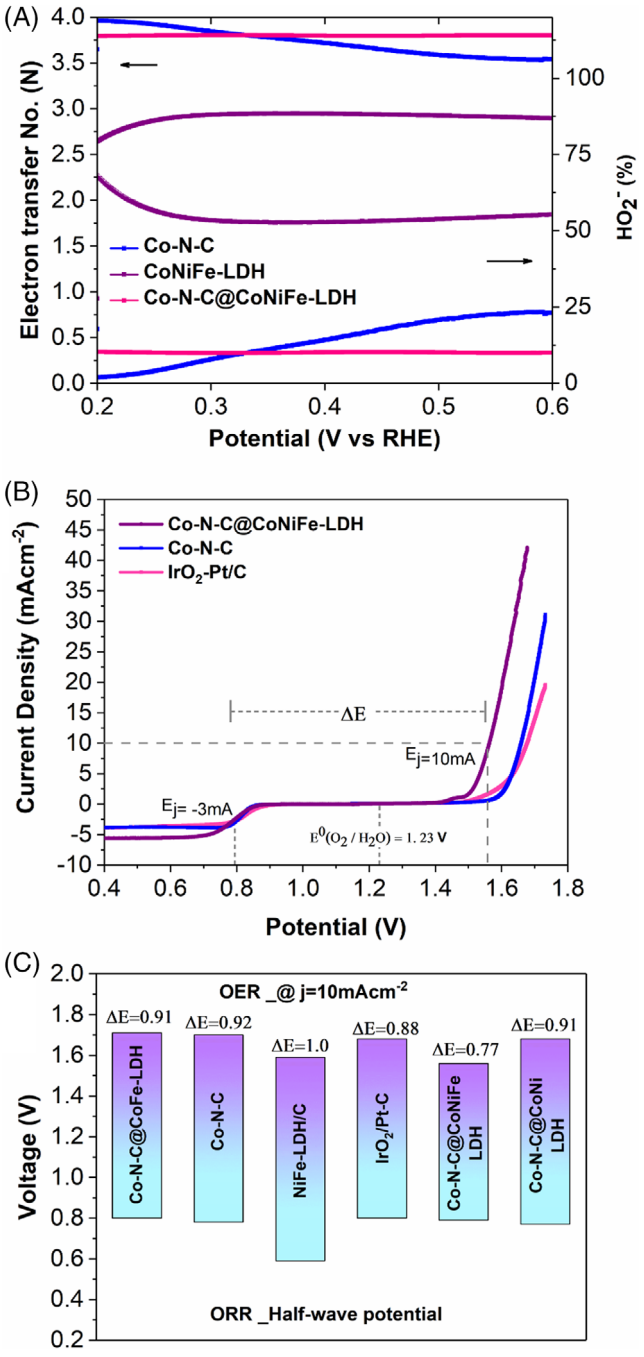

FIGURE 5 (A) Electron transfer number (N) and HO^{2-} yield (%), (B) overall polarization curves of the catalysts Co-N-C@C0FeNi-LDH, Co-N-C and Pt/C and IrO_2 in alkaline solution (0.1 M KOH), (C) ΔE, obtained through various catalysts.

responsible for achieving the high current density at low overpotential. The electrochemical double layer capacitance (C_{dl}) was evaluated using cyclic voltammetry (CV) in the non-Faradaic range at several scan rates (Figure S7a,b). It can be visualized that C_{dl} of Co-N-C@CoNiFe-LDH is 4.8 mF cm^{-2}, which is superior to that of pristine NiFe-LDH.[35,36] It confirms that Co-N-C@CoNiFe-LDH possesses the high specific surface area

which is in line with BET surface area. The electrochemical durability of the optimal catalyst was evaluated using chronoamperometric response and accelerated cyclic voltammetry (CV) as shown in Figure S8. After 15 h measurement and 1000 CV cycles, there was a negligible decline in the OER activity, revealing an excellent stability of Co-N-C@CoNiFe-LDH.

Similarly, ORR activity was evaluated by measuring the half-wave potential as illustrated in Figures 4C and S9. The ORR activity of Co-N-C@ CoNiFe-LDH was comparable to the Co-N-C, a well-known carbon-based catalyst with high ORR activity. Interestingly, the limiting current density was significantly larger than the Co-N-C and precious metal-based Pt/C catalyst, which may be associated with the improvement in the electronic conductivity as a result of the formation of ternary LDH after the incorporation of Co into the NiFe-LDH. Besides, N-doped carbon significantly contributed to the effective electronic transportation. Moreover, N species offered additional positive sites for optimizing the adsorption capacity of oxygen intermediates and increasing the overall catalytic performance.[37,38] For comparison, ORR activities of pristine NiFe-LDH, Co-N-C@CoFe-LDH, and Co-N-C@CoNi-LDH were also presented, which were far less as opposed to Co-N-C@ CoNiFe-LDH (Figure S6). The electrochemical durability of Co-N-C (ORR active sites) was also estimated using chronoamperometric response and accelerated cyclic voltammetry (CV) as shown in Figure S10. It can be noticed that there was a negligible decline in the ORR activity over a period of 15 h and 1000 CV cycles, implying the excellent ORR stability of Co-N-C.

The rotating ring-disk electrode was further utilized to ascertain the ORR mechanism as shown in Figure 5A. We calculated the peroxide yield in percentage and electron transfer numbers of the catalysts. It can be observed that CoNiFe-LDH catalyst underwent approximately $3e^-$ pathway and the peroxide yield was more than 50%. However, when CoNiFe-LDH was grown on Co-N-C, it presented a stable electron transfer number, approaching $4e^-$, together with a less amount of peroxide yield over a whole potential range. It implies that the peroxide intermediates were rapidly reduced in the presence of Co-N-C. Thus, the reduction ability of H_2O_2 was significantly improved followed by the growth of CoNiFe-LDH over Co-N-C, which is aligned with the literature.[39] Interestingly, the optimal catalyst was found more selective even superior to that of Co-N-C.

The bifunctional activity parameter ΔE, (the differences in $E_j = 10$ and -3 mA cm^{-2}) of Co-N-C@ CoNiFe-LDH was then evaluated (Figure 5B,C). A lesser value of ΔE indicates a smaller energy loss and eventually a higher electrochemical activity. Clearly, it can be visualized that the optimal catalyst possessed excellent bi-functional activity ($\Delta E = 0.77$ V). Interestingly, its bifunctionality even outperformed the precious metal-based benchmarks. Such high performance may also be credited to the more exposed LDHs sites from the highly mesoporous Co-N-C network. Moreover, their intimate contact also reduced the interfacial resistance, building efficient ionic and electronic pathways for rapid electronic transport and mass diffusivity during the redox reactions.[40,41]

2.3 | Zinc-air battery performance

Considering its promising physicochemical and electrochemical properties, the Co-N-C@CoNiFe-LDH catalyst was further integrated into ZABs. Co-N-C@ CoNiFe-LDH and precious metal-based (IrO_2/Pt-C) catalysts as air cathodes, were employed into ZABs operating in the ambient air (Figure 6A). The ZAB with the Co-N-C@ CoNiFe-LDH air electrode displayed a high open circuit voltage of 1.48 V (Figure 6B). In addition, it showed excellent performance while charging and discharging, leading to a low charging-discharging potential gap of 0.77 V at 5 mA cm^{-2} (Figure 6C). It delivered a high PPD of 228 mW cm^{-2} in the discharging process (Figure 6D), and demonstrated a stable performance over 950 h. In contrast, the performance of the ZAB with the precious metal-based IrO_2/Pt-C battery started to decline even after a few hours of operation. As shown in Figure S11, the ZAB with the ZIF-67-derived Co-N-C catalyst exhibited a large potential gap of 0.91 V at similar conditions. Furthermore, the PPD and cycling stability of the optimal catalyst were compared with the recently reported non-precious metal-based air electrodes in the rechargeable ZABs (Figure 6E and Table S2). It is worth noticing that Co-N-C@ CoNiFe-LDH catalyst displayed superior performance to the most of reported catalysts. Thus, it can be concluded that Co-N-C@ CoNiFe-LDH catalyst is a superior bi-functional air electrode for ZABs. Interestingly, when the optimal catalyst was tested at higher current density (i.e. 10 mA cm^{-2}), it also presented the excellent performance with a low charging-discharging potential gap over a period of 500 h (Figure S12).

The outstanding bi-functional activity together with the stability of Co-N-C@ CoNiFe-LDH may be linked with the synergistic effect of in situ generated ternary CoNiFe-LDH and ZIF-67 derived Co-N-C (Figure 7). In particular, CoNiFe-LDH contributed to the OER activity. As (oxy)hydroxides, recognized as the crucial OER intermediates, function as the active sites, responsible for the generation of oxygen. Therefore, Fe reduction significantly promoted the oxidation reaction of Ni^{2+}/Ni^{3+} and

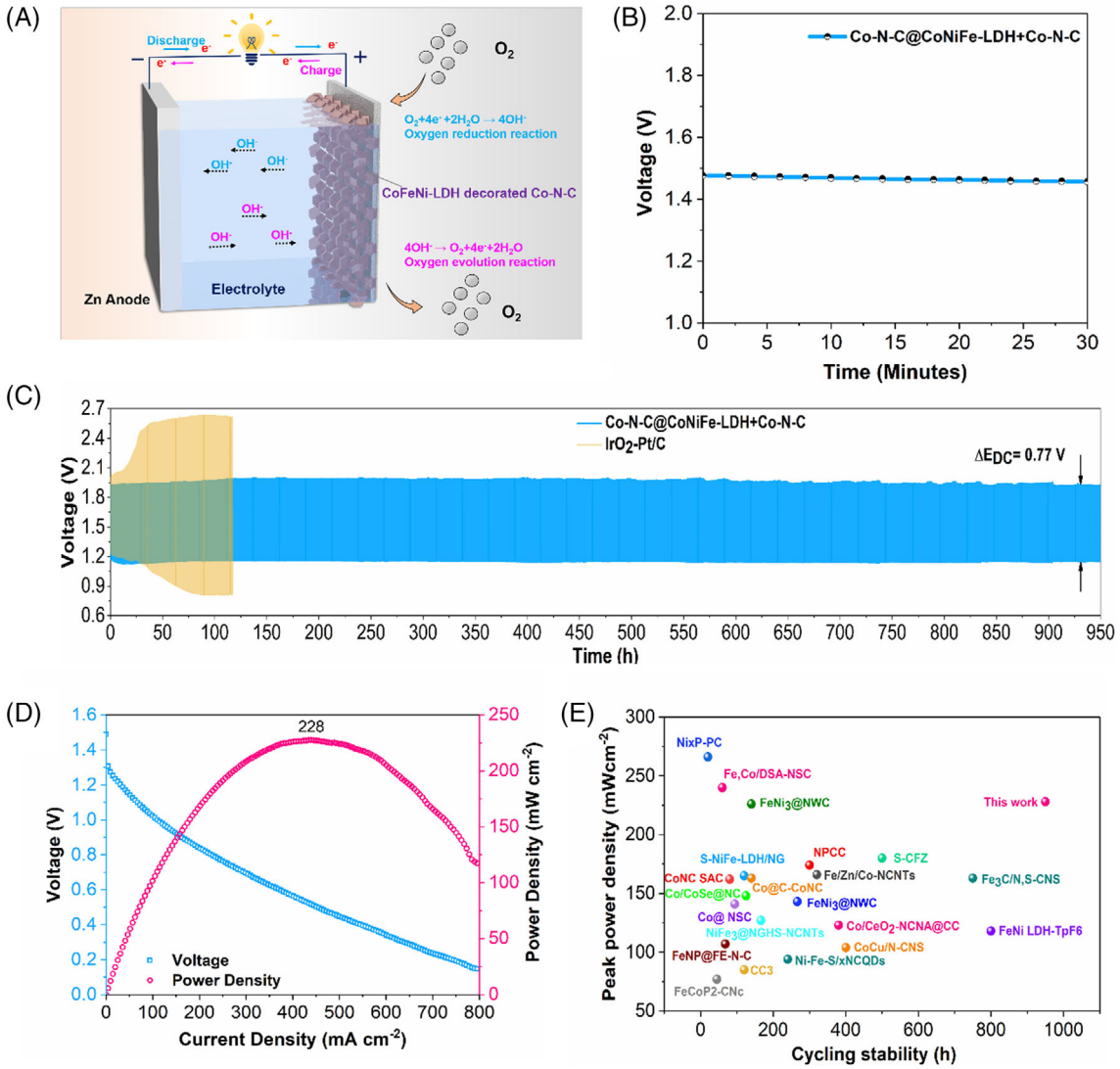

FIGURE 6 (A) Open-circuit voltage, (B) voltage and power density plots, (C) galvanostatic charging-discharging for Co-N-C@CoNiFe-LDH + Co-N-C (3:1) and IrO_2_Pt/C catalysts at 5 mA cm^{-2} for 950 h.

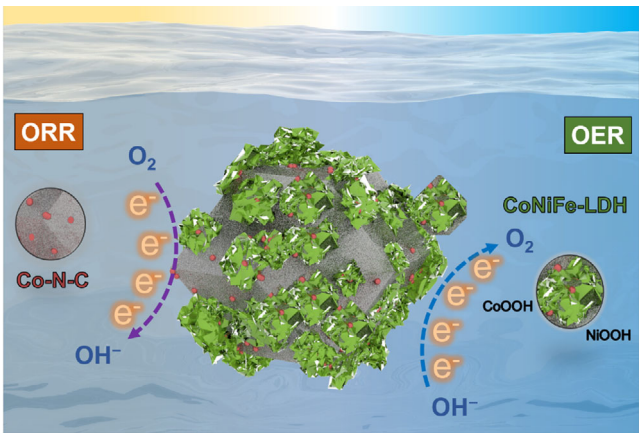

FIGURE 7 Schematic illustrates the Co-N-C and Co-N-C@CoNiFe-LDH active sites for oxygen reduction reaction and oxygen evolution reaction, respectively.

Co^{2+}/Co^{3+}wherein Fe^{3+} can fine-tune the valence state, for instance, Ni^{2+} [$Ni(OH)_2$] to Ni^{3+} [NiOOH].[42] Actually, the electron trapping or electron withdrawing effect of Fe^{3+} induced the high valence states of Ni^{3+} and Co^{3+} species by the partial-charge transfer activation and served as the real active sites for the absorption of OH. Thus, Fe^{3+} tends to partially reduce during the polarization and leading to the generation of NiOOH and CoOOH active centers.[42–44] Moreover, the interaction between Ni/Co and Fe atoms is likely to stabilize the OER intermediates (*OH, *O and *OOH) wherein OH^- adsorption is thermodynamically favorable at Fe sites whereas the deprotonation of *OOH for the evolution of O_2 molecules is feasible at Ni/Co sites.[38,45,46] Moreover, Co-N-C supplied the trivalent cobalt ions (Co^{3+}) to NiFe-LDH. The incorporation of Co ions into NiFe-LDH stabilized the local coordination environment of Fe and aided

the π-symmetry bonding orbital in CoNiFe-LDH.[34] Also, cobalt co-ordinated, and N-doped carbon network accelerated the evolution of metal (CoNiFe) OOH active sites, which provided an opportunity to optimize the binding energies for OER intermediates and eventually improved the overall OER kinetics (Figure S13). Furthermore, the more positively charged Co^{3+} species in the intralayer of the CoNiFe-LDH may augment the more electrophilicity of the adsorbed O atoms, promoting the formation of OOH species. As a result, the incorporation of cobalt ions into the LDH structure modulated the electronic structure, enhancing the intrinsic OER activity.

ZIF-67 derived Co-N-C, on the other hand, endowed the excellent ORR activity. N-heteroatom doping induced the net positive charge on the carbon atoms.[47] It is deemed as lucrative for oxygen adsorption and O-O bond breaking, promoting ORR activity. Co-N-C also significantly contributed to enhance the electrical conductivity, while efficient charge transport is essential for the excellent ORR and OER activities. Thereby, ZIF-67 served as not only the additive to provide the active sites to CoNiFe-LDH but also a template and contributed to ORR activity and electrical conductivity. As a result, the optimal catalyst Co-N-C@ CoNiFe-LDH exhibited both excellent activity and outstanding stability.

3 | CONCLUSIONS

In conclusion, we have successfully synthesized a bi-functional oxygen electrocatalyst by the in-situ development of ternary CoNiFe-LDH over cobalt co-ordinated, N-doped porous carbon framework via hydrothermal treatment. Their symbiotic interaction modulated the atomic and electronic structure at the heterostructure. Moreover, the introduction of Co species into NiFe-LDH enhanced the electrical conductivity and lowered the onset potential for OER. On the other hand, Co-N-C network not only contributed to enhancing the electrical conductivity but also offered excellent ORR activity. As a result, CoNiFe-LDH endowed the OER activity whereas Co-N-C porous carbon network delivered the ORR activity. Moreover, the in situ development of CoNiFe-LDH over Co-N-C provided the intimate contact and structural robustness. Subsequently, interfacial resistance was tangibly suppressed, promoting ionic diffusivity as well as the electronic conductivity. Consequently, Co-N-C@ CoNiFe-LDH catalyst requires only 1.540 V to reach 10 mA cm^{-2} in alkaline media (0.1 M KOH). When Co-N-C@CoNiFe-LDH air cathode was integrated into zinc-air batteries, it exhibited excellent activity, demonstrating a low charging-discharging voltage gap of 0.77 V at 5 mA cm^{-2}, ultra-long stability over 950 h and high PPD of 228 mW cm^{-2}. This unique and facile synthesis strategy paves the way for designing the bi-functional electrocatalysts by utilizing the heterostructure engineering for various catalysis applications.

3.1 | Experimental section

3.1.1 | Synthesis of ZIF-67-derived Co-N-C

ZIF-67 was synthesized by employing $Co(NO_3)_2{\cdot}6H_2O$, 2-methylimidazole (2-MIM) as raw materials, methanol as solvent and Pluronic F-127 as a surfactant. For a typical synthesis, 1.426 g $Co(NO_3)_2.6H_2O$ and 1.50 g of surfactant were dissolved in 50 mL of methanol solvent. Similarly, a solution consisting of 1.50 g 2-MIM, and 50 mL of solvent (methanol) was prepared separately. The pink solution of metal salt was then poured slowly into the 2-MIM solution of organic ligand, which was continuously stirred till crystallization occurred. The ZIF-67 crystals were filtered and dried at 120°C, which was further pyrolyzed at 920°C for 2 h in flowing N_2 in a tube furnace to derive the porous Co-N-C metal-doped carbon material.

3.1.2 | Synthesis of Co-N-C@ CoNiFe-LDH

Co-N-C@ CoNiFe-LDH was synthesized by in-situ growth of NiFe-LDH on Co-N-C substrate via a facile hydrothermal method. Typically, 0.5 mmol of $Fe(NO_3)_3{\cdot}9H_2O$ and $Ni(NO_3)_2{\cdot}6H_2O$ each together with 5 mmol of urea were dissolved in 36 mL of distilled water under continuous stirring till a clear solution was obtained. Then 50 mg of as-prepared Co-N-C sample was mixed into the solution, while continuously stirring for another 15 minutes. The aqueous solution consisting of LDH precursors and Co-N-C substrate was transferred to an autoclave reactor with a Teflon lining. The autoclave was placed in the oven at 120°C for 14 h. After cooling to room temperature, the product was rinsed with distilled solvents such as distilled water and ethanol respectively for 5 min, followed by centrifugation, filtering and drying at 60°C for few hours. For the sake of comparison, three other products were also synthesized by following the same procedure: $Fe(NO_3)_3{\cdot}9H_2O$ and Co-N-C substrate (named as Co-N-C@CoFe-LDH); $Ni(NO_3)_2{\cdot}6H_2O$ and Co-N-C substrate (named as Co-N-C@CoNi-LDH) and pristine NiFe-LDH without adding Co-N-C substrate. For the synthesis of pristine CoNiFe-LDH, Co salt precursor (20% mole ratio of Ni) was added in the NiFe-LDH synthesis process.

3.2 | Characterizations

XRD, TEM, and SAED were conducted to analyze the crystal phases of the samples, which were conducted using D8 Discover (Bruker AXS, Cu Kα radiation) and FEI Talos (FS200X G2), respectively. The elemental dispersion of the materials was observed by EDS mapping using FEI Talos. Morphologies of the electrocatalysts were visualized using scanning electron microscopy (TESCAN MIRA) and TEM (FEI Talos). Specific surface area, porosity and pore structure of the electrocatalysts were measured by the N_2 adsorption/desorption isotherms method with Micrometrics Tristar II plus by employing ASAP 2020 HD88 equipment at 77 K and were computed by employing the BET theory. The oxidation states of the electrocatalysts were characterized by utilizing X-ray photoelectron spectroscopy using Kratos AXIS Ultra DLD (Al Kα radiation).

3.3 | Electrochemical tests

OER and ORR catalytic activities of the materials were examined based on the rotation disk electrode in a three-electrode glass assembly, comprising a working electrode (glassy carbon, diameter: 5 mm), a reference electrode (Ag/AgCl), and a counter electrode (platinum spiral) in an alkaline solution (0.1 M KOH). The ink based on samples was prepared by mixing the 10 mg of sample in 1 mL of ethanol, and 0.1 mL of 5% Nafion 117 for an hour in an ultrasonic bath. Then, 5 μL of ink based on samples was cast dropwise on the working electrode. Linear sweep voltammetry was acquired at a scan rate of 5 mV s^{-1} using a bipotentiostat (CHI760E, USA) and the rotation speed of the disc was adjusted at 1600 rpm. On the other hand, the rotating ring-disk electrode was applied to quantify the peroxide formation (%) as well as the electron transfer number (n). In this case, the working electrode consists of two concentric rings: a disc (diameter: 5.61 mm) surrounded by a platinum ring (diameter: 6.25 mm).

The measurement of potential was conducted against Ag/AgCl electrode and subsequently transformed into the potentials based on reversible hydrogen electrode (RHE) by the following equation:

$$E_{\mathrm{RHE}} = E\left(\frac{\mathrm{Ag}}{\mathrm{AgCl}}\right) + 0.199 + 0.0591 \times \mathrm{pH}. \quad (5)$$

Similarly, the estimation of electron transfer number (n) and the yield of peroxide (%) were made by following Equations (6) and (7)

$$n = 4 \times \frac{I_d}{\left(I_d + \frac{I_r}{N}\right)}, \quad (6)$$

$$\mathrm{HO_2^-}\ (\%) = 200 \times \frac{\frac{I_r}{N}}{\left(I_d + \frac{I_r}{N}\right)}. \quad (7)$$

The electrical double-layer capacitance was calculated by cyclic voltammetry with scan rate ranging from 5 to 100 mV s^{-1} in non-Faradaic potential region (0.967–1.067 V vs. RHE).

Zn-air batteries assembly and performance evaluation.

ZABs were assembled by employing the basic components: zinc anode, alkaline electrolyte consisting of 6 M KOH and 0.2 M $Zn(Ac)_2$ and air electrode. To prepare the air cathode, the same ink was cast dropwise on the carbon cloth on gas diffusion layer to end up a mass loading of 2 mg cm^{-2}. Subsequently, the long-term battery charging/discharging performance was appraised using LANHE CT2001A battery testing system, whereas other electrochemical assessments were recorded using VSP Biologic potentiostat.

AUTHOR CONTRIBUTIONS

Yasir Arafat: Conceptualization, acquisition of data, formal analysis, investigation, methodology, software, visualization and writing-original draft. **Yijun Zhong:** Acquisition of data, investigation, methodology, software and validation. **Muhammad R. Azhar:** Acquisition of data, interpretation of data, formal analysis, investigation, methodology, software and validation. **Mohammad Asif:** Interpretation of data, software, validation, and revision. **Moses O. Tadé:** Supervision, visualization, validation, resources, and revision. **Zongping Shao:** Conceptualization, visualization, validation, project administration, resources, supervision and writing – review & editing.

ACKNOWLEDGMENTS

The authors would like to acknowledge the financial supports from Australian Research Council Discovery Projects via grant Nos. DP220103669, DP200103332, and DP200103315.

CONFLICT OF INTEREST STATEMENT

The authors declare no conflict of interest.

ORCID

Mohammad Asif https://orcid.org/0000-0003-3196-0074

Zongping Shao https://orcid.org/0000-0002-4538-4218

REFERENCES

1. Arafat Y, Azhar MR, Zhong Y, Xu X, Tadé MO, Shao Z. A porous nano-micro-composite as a high-performance bi-functional air

electrode with remarkable stability for rechargeable zinc–air batteries. *Nano-Micro Lett*. 2020;12(1):130. doi:10.1007/s40820-020-00468-4

2. Al-Fatesh AS, Arafat Y, Kasim SO, Ibrahim AA, Abasaeed AE, Fakeeha AH. In situ auto-gasification of coke deposits over a novel Ni-Ce/W-Zr catalyst by sequential generation of oxygen vacancies for remarkably stable syngas production via CO_2-reforming of methane. *Appl Catal B*. 2021;280:119445. doi:10.1016/j.apcatb.2020.119445
3. Hodgkinson JH, Smith MH. Climate change and sustainability as drivers for the next mining and metals boom: the need for climate-smart mining and recycling. *Resources Policy*. 2021;74:101205. doi:10.1016/j.resourpol.2018.05.016
4. Arafat Y, Azhar MR, Zhong Y, O'Hayre R, Tadé MO, Shao Z. Organic ligand-facilitated in situ exsolution of CoFe alloys over $Ba_{0.5}Sr_{0.5}Co_{0.8}Fe_{0.2}O_{3-\delta}$ perovskite toward enhanced oxygen electrocatalysis for rechargeable Zn-air batteries. *J Mater Chem A*. 2023;11:12856-12865. doi:10.1039/D2TA07104E
5. Colglazier W. Sustainable development agenda: 2030. *Science*. 2015;349(6252):1048-1050. doi:10.1126/science.aad2333
6. Cai C, Wang M, Han S, et al. Ultrahigh oxygen evolution reaction activity achieved using Ir single atoms on amorphous CoO_x nanosheets. *ACS Catal*. 2020;11(1):123-130. doi:10.1021/acscatal.0c04656
7. Yang Z, Xiang M, Zhu Y, et al. Single-atom platinum or ruthenium on C_4N as 2D high-performance electrocatalysts for oxygen reduction reaction. *Chem Eng J*. 2021;426:131347. doi:10.1016/j.cej.2021.131347
8. Lv L, Yang Z, Chen K, Wang C, Xiong Y. 2D layered double hydroxides for oxygen evolution reaction: from fundamental design to application. *Adv Energy Mater*. 2019;9(17):1803358. doi:10.1002/aenm.201803358
9. Lu Z, Xu W, Zhu W, et al. Three-dimensional NiFe layered double hydroxide film for high-efficiency oxygen evolution reaction. *Chem Commun*. 2014;50(49):6479-6482. doi:10.1039/C4CC01625D
10. Song F, Hu X. Exfoliation of layered double hydroxides for enhanced oxygen evolution catalysis. *Nat Commun*. 2014;5(1):4477. doi:10.1038/ncomms5477
11. Wang Y, Yan D, El Hankari S, Zou Y, Wang S. Recent progress on layered double hydroxides and their derivatives for electrocatalytic water splitting. *Adv Sci*. 2018;5(8):1800064. doi:10.1002/advs.201800064
12. Tan C, Cao X, Wu X-J, et al. Recent advances in ultrathin two-dimensional nanomaterials. *Chem Rev*. 2017;117(9):6225-6331. doi:10.1021/acs.chemrev.6b00558
13. Yu J, Wang Q, O'Hare D, Sun L. Preparation of two dimensional layered double hydroxide nanosheets and their applications. *Chem Soc Rev*. 2017;46(19):5950-5974. doi:10.1039/C7CS00318H
14. Long X, Wang Z, Xiao S, An Y, Yang S. Transition metal based layered double hydroxides tailored for energy conversion and storage. *Mater Today*. 2016;19(4):213-226. doi:10.1016/j.mattod.2015.10.006
15. Guo P-F, Yang Y, Wang W-J, et al. Stable and active NiFeW layered double hydroxide for enhanced electrocatalytic oxygen evolution reaction. *Chem Eng J*. 2021;426:130768. doi:10.1016/j.cej.2021.130768
16. Yang Y, Dang L, Shearer MJ, et al. Highly active trimetallic NiFeCr layered double hydroxide electrocatalysts for oxygen evolution reaction. *Adv Energy Mater*. 2018;8(15):1703189. doi:10.1002/aenm.201703189
17. Zou X, Goswami A, Asefa T. Efficient noble metal-free (electro) catalysis of water and alcohol oxidations by zinc–cobalt layered double hydroxide. *J Am Chem Soc*. 2013;135(46):17242-17245. doi:10.1021/ja407174u
18. Song F, Hu X. Ultrathin cobalt–manganese layered double hydroxide is an efficient oxygen evolution catalyst. *J Am Chem Soc*. 2014;136(47):16481-16484. doi:10.1021/ja5096733
19. Wang A-L, Xu H, Li G-R. NiCoFe layered triple hydroxides with porous structures as high-performance electrocatalysts for overall water splitting. *ACS Energy Lett*. 2016;1(2):445-453. doi:10.1021/acsenergylett.6b00219
20. Ma W, Ma R, Wang C, et al. A superlattice of alternately stacked Ni–Fe hydroxide nanosheets and graphene for efficient splitting of water. *ACS Nano*. 2015;9(2):1977-1984. doi:10.1021/nn5069836
21. Long X, Li J, Xiao S, et al. A strongly coupled graphene and FeNi double hydroxide hybrid as an excellent electrocatalyst for the oxygen evolution reaction. *Angew Chem Int*. 2014;53(29):7584-7588. doi:10.1002/anie.201402822
22. Park YS, Jeong J-Y, Jang MJ, et al. Ternary layered double hydroxide oxygen evolution reaction electrocatalyst for anion exchange membrane alkaline seawater electrolysis. *J Energy Chem*. 2022;75:127-134. doi:10.1016/j.jechem.2022.08.011
23. Wang T, Xu W, Wang H. Ternary NiCoFe layered double hydroxide nanosheets synthesized by cation exchange reaction for oxygen evolution reaction. *Electrochim Acta*. 2017;257:118-127. doi:10.1016/j.electacta.2017.10.074
24. Qian L, Lu Z, Xu T, et al. Trinary layered double hydroxides as high-performance bifunctional materials for oxygen electrocatalysis. *Adv Energy Mater*. 2015;5(13):1500245. doi:10.1002/aenm.201500245
25. Arafat Y, Zhong Y, Tadé MO, Shao Z. Design of three-dimensional air cathode in zinc–air batteries. In: Shao Z, Xu X, eds. *Zinc-Air Batteries: Introduction, Design Principles and Emerging Technologies*. Wiley-VCH GmbH; 2022:111-154. doi:10.1002/9783527837939.ch4
26. Arafat Y, Azhar MR, Zhong Y, Abid HR, Tadé MO, Shao Z. Advances in zeolite imidazolate frameworks (ZIFs) derived bifunctional oxygen electrocatalysts and their application in zinc–air batteries. *Adv Energy Mater*. 2021;11(26):2100514. doi:10.1002/aenm.202100514
27. Zhong Y, Xu X, Liu Y, Wang W, Shao Z. Recent progress in metal–organic frameworks for lithium–sulfur batteries. *Polyhedron*. 2018;155:464-484. doi:10.1016/j.poly.2018.08.067
28. Fatima H, Azhar MR, Zhong Y, Arafat Y, Khiadani M, Shao Z. Rational design of ZnO-zeolite imidazole hybrid nanoparticles with reduced charge recombination for enhanced photocatalysis. *J Colloid Interface Sci*. 2022;614:538-546. doi:10.1016/j.jcis.2022.01.086
29. Zhong Y, Xu X, Wang W, Shao Z. Recent advances in metal-organic framework derivatives as oxygen catalysts for zinc-air batteries. *Batteries Supercaps*. 2019;2(4):272-289. doi:10.1002/batt.201800093
30. Jiang Z, Li Z, Qin Z, Sun H, Jiao X, Chen D. LDH nanocages synthesized with MOF templates and their high performance as supercapacitors. *Nanoscale*. 2013;5(23):11770-11775. doi:10.1039/c3nr03829g

31. Sun S, Li H, Xu ZJ. Impact of surface area in evaluation of catalyst activity. *Joule*. 2018;2(6):1024-1027. doi:10.1016/j.joule.2018.05.003
32. Li J-G, Sun H, Lv L, et al. Metal–organic framework-derived hierarchical (Co, Ni) Se_2@NiFe LDH hollow nanocages for enhanced oxygen evolution. *ACS Appl Mater Interfaces*. 2019;11(8):8106-8114. doi:10.1021/acsami.8b22133
33. Bates MK, Jia Q, Doan H, Liang W, Mukerjee S. Charge-transfer effects in Ni–Fe and Ni–Fe–Co mixed-metal oxides for the alkaline oxygen evolution reaction. *ACS Catal*. 2016;6(1):155-161. doi:10.1021/acscatal.5b01481
34. Lin Y, Wang H, Peng C-K, et al. Co-induced electronic optimization of hierarchical NiFe LDH for oxygen evolution. *Small*. 2020;16(38):2002426. doi:10.1002/smll.202002426
35. Park KR, Jeon J, Choi H, et al. NiFe layered double hydroxide electrocatalysts for an efficient oxygen evolution reaction. *ACS Appl Energy Mater*. 2022;5(7):8592-8600. doi:10.1021/acsaem.2c01115
36. Cai S, Liu H, Cheng H, et al. Deeply reconstructed NiFe layered double hydroxide nanosheets for an efficient oxygen evolution reaction. *ACS Appl Nano Mater*. 2023;6(9):7864-7872. doi:10.1021/acsanm.3c01002
37. Dionigi F, Strasser P. NiFe-based (oxy) hydroxide catalysts for oxygen evolution reaction in non-acidic electrolytes. *Adv Energy Mater*. 2016;6(23):1600621. doi:10.1002/aenm.201600621
38. Wang R, Liu J, Xie J, et al. Hollow nanocage with skeleton Ni-Fe sulfides modified by N-doped carbon quantum dots for enhancing mass transfer for oxygen electrocatalysis in zinc-air battery. *Appl Catal B*. 2023;324:122230. doi:10.1016/j.apcatb.2022.122230
39. Gong K, Du F, Xia Z, Durstock M, Dai L. Nitrogen-doped carbon nanotube arrays with high electrocatalytic activity for oxygen reduction. *Science*. 2009;323(5915):760-764. doi:10.1126/science.1168049
40. Huang Y, Liu X, Li X, et al. Interfacial oxidation using potassium ferrate to fabricate self-supported hydrophilic NiFe-LDH nanoarrays for overall water splitting at high current density. *Sustainable MaterTechnol*. 2022;34:e00508. doi:10.1016/j.susmat.2022.e00508
41. Ko T-E, Hosseini S, Tseng C-M, Tsai J-E, Wang W-H, Li Y-Y. Tetrafunctional electrocatalyst for oxygen reduction, oxygen evolution, hydrogen evolution, and carbon dioxide reduction reactions. *J Taiwan Inst Chem Eng*. 2022;136:104397. doi:10.1016/j.jtice.2022.104397
42. Trotochaud L, Young SL, Ranney JK, Boettcher SW. Nickel–iron oxyhydroxide oxygen-evolution electrocatalysts: the role of intentional and incidental iron incorporation. *J Am Chem Soc*. 2014;136(18):6744-6753. doi:10.1021/ja502379c
43. Parvin S, Chaudhary DK, Ghosh A, Bhattacharyya S. Attuning the electronic properties of two-dimensional Co-Fe-O for accelerating water electrolysis and photolysis. *ACS Appl Mater Interfaces*. 2019;11(34):30682-30693. doi:10.1021/acsami.9b05294
44. Huang F, Yao B, Huang Y, Dong Z. NiFe layered double hydroxide nanosheet arrays for efficient oxygen evolution reaction in alkaline media. *Int J Hydrog Energy*. 2022;47(51):21725-21735.
45. Li X, Liu Y, Chen H, et al. Rechargeable Zn–air batteries with outstanding cycling stability enabled by ultrafine FeNi nanoparticles-encapsulated N-doped carbon nanosheets as a bifunctional electrocatalyst. *Nano Lett*. 2021;21(7):3098-3105. doi:10.1021/acs.nanolett.1c00279
46. Lu XF, Fang Y, Luan D, Lou XWD. Metal–organic frameworks derived functional materials for electrochemical energy storage and conversion: a mini review. *Nano Lett*. 2021;21(4):1555-1565. doi:10.1021/acs.nanolett.0c04898
47. Arafat Y, Azhar MR, Zhong Y, Tadé MO, Shao Z. Metal-free carbon based air electrodes for Zn-air batteries: recent advances and perspective. *Mater Res Bull*. 2021;140:111315. doi:10.1016/j.materresbull.2021.111315

SUPPORTING INFORMATION

Additional supporting information can be found online in the Supporting Information section at the end of this article.

How to cite this article: Arafat Y, Zhong Y, Azhar MR, Asif M, Tadé MO, Shao Z. CoNiFe-layered double hydroxide decorated Co-N-C network as a robust bi-functional oxygen electrocatalyst for zinc-air batteries. *EcoMat*. 2023;5(10):e12394. doi:10.1002/eom2.12394